VIII International Conference on Computational Methods in Marine Engineering
MARINE 2019
R. Bensow and J. Ringsberg (Eds)

EULERIAN-LAGRANGIAN SIMULATION ON MICROBUBBLES IN TURBULENT CHANNEL FLOW

XIAOSONG ZHANG, JIANHUA WANG AND DECHENG WAN*

Collaborative Innovation Center for Advanced Ship and Deep-Sea Exploration, State Key Laboratory of Ocean Engineering, School of Naval Architecture, Ocean and Civil Engineering, Shanghai Jiao Tong University, Shanghai, China
*Corresponding author: dcwan@sjtu.edu.cn

Key words: Microbubbles; Euler-Lagrange method; Turbulent channel flow; Drag reduction

Abstract. Microbubble drag reduction technology has been proved by many experiments that it can reduce frictional resistance of ships significantly. The underlying physical mechanism of drag reduction needs to be studied by means of numerical simulation. In this paper, Eulerian-Lagrangian method is used to study the interaction between microbubbles and a fully developed turbulent channel flow. Turbulent flow field is solved using large eddy simulation (LES) method. The microbubble trajectories were tracked by the motion equation following Newton's second law in Lagrangian framework. The interaction between microbubbles and liquid is fully considered in the simulation. The computational code is developed based on the open-source platform OpenFOAM. Before introducing bubbles, a fully developed single-phase turbulent channel flow is obtained at friction Reynolds number. The mean streamwise velocity, turbulent normal and shear stresses are verified by comparison with standard DNS results. Microbubbles are injected uniformly into the channel and eventually form a bubble layer on the upper plate due to buoyancy. The drag reduction of the upper plate is calculated and detailed analysis is carried out about the interaction between microbubbles and turbulent boundary layer.

1 INTRODUCTION

During the past several years, reducing ship resistance has become one of the most important objectives of ship research. It has been reported that skin frictional resistance accounts for as much as 60%-70% of the total drag for cargo ship, and about 80% of that for a tanker. Therefore, reducing frictionl resistance is an important way to save cost in shipping industry in the marine transportation business[1]. Microbubble drag reduction technology takes advantage of blower and porous plate to inject microbubbles to the bottom of ship, which can significantly reduce frictional resistance. In order to investigate the underlying physical mechanism. Many scholars simplified the bottom plate of a ship into a flat plate and studied the interaction between microbubbles and the flow field around the plate.

Madavan et al.[2-3] and Merkle et al.[4] carried out experimental studies on the microbubble drag reduction in a channel very early. Drag reduction effect was obtained under different air flow rate. Their analysis showed that the region where the bubbles mainly acted on the fluid was in the turbulent boundary layer, rather than the fluid outside the boundary layer. A series

of bubble drag reduction experiments[5-7] were carried out on a long plate in in the USA Navy's Large Cavitation Channel. The experiment results showed that bubbles tend to concentrate on the plate and the highest drag reduction rate can be up to 90% under the low velocity condition. These experiments confirm the drag reduction effect of the microbubble drag reduction technology.

However, it is difficult to extract and analyze the detailed flow information in the experiment. Thus, CFD method is needed to investigate the deep mechanism. Eulerian-Eulerian and Eulerian-Lagrangian are two methods that are mostly used to simulate the fluid carried discrete bubbles. Eulerian-Eulerian method means that liquid and bubble are both solved under Eulerian framework, whose most prominent advantage is the low computational cost. Kunz et al.[8-9] developed an Eulerian-Eulerian code for the modeling of high Reynolds number external flows with microbubble drag reduction, the code has been validated by comparison with experimental results that it can predict drag reduction effect correctly across a wide range of Reynolds numbers. Qin et al.[10] combine the CFD method in Eulerian framework with population balance model (PBM) to simulate the bubbly flow. The PBM method was used to predit the coalescence and breakup of bubbles. The numerical results were qualitatively correct compared with the experimental results. The Eulerian-Eulerian method can be used in industrial applications because of the lower expense, but detailed behavior of bubbles cannot be resolved. To get more accurate results, many scholars use Eulerian-Lagrangian method for mechanism investigation. In this method, the bubble motion is obtained by solving the kinetic equation in the Lagrangian framework. Xu et al.[11] firstly carried out numerical simulation of drag reduction of microbubbles in a channel flow. Bubbles were tracking using Lagrangian method and fluid was solved using Driect Numerical Simulation (DNS) method. Their results proved that smaller bubbles have a greater impact on turbulent flow. The same method was used by Ferrante et al.[12] to investigate the mechanism for drag reduction in a microbubble ladened turbulent boundary layer over a flat plate. Early studies often made a lot of simplifying assumptions such as ignoring bubble gravity and buoyancy, bubble free from collide. The number of bubbles were also relatively small. More recently, Pang et al.[13] used two-way coupling Eulerian-Lagrangian method to study the interaction between microbubbles and liquid turbulence with the help of interphase forces in channel flow. Asiagbe et al.[14] also carried out bubbly channel flow simulation, specially, they adopt Large Eddy Simulation (LES) method to solve the fluid. In contrast with DNS method, LES method requires less computing resources and can also reasonably reproduce the bubble-induced velocity fluctuations in the liquid. The uses of LES makes it possible to study drag reduction at high Reynolds number and bubble fraction. In the previous studies, simulation of microbubbles is highly simplified. Interaction between microbubble was usually ignored[13] or was described by simple hard sphere model[14]. Soft sphere model is used to simulate bubble interaction in this paper in order to simulate the bubble-bubble interaction and bubble-wall interaction more veritably.

The present paper is organized as follows. The numerical method is presented at first including liquid phase solving and discrete phase solving. The computational conditions are introduced next. Computational results for single phase turbulent flow and bubbly flow are shown in the simulation part, where the impact of microbubbles on the mean velocity profile, turbulent intensities and Reynolds stress are analyzed in detial. A brief conclusion is given in the end.

2 NUMERICAL METHOD

In Eulerian-Lagrangian method, liquid phase and discrete phase are treated in different frameworks. In this paper, the fluid is solved using LES method in Eulerian framework, while microbubbles are tracked by the motion equation following Newton's second law. The coupling between two phases is considered by interphase interaction forces, which are described as momentum source term of the momentum equation. For the liquid-phase calculation, temporal discretization adopts a second-order implicit scheme, and second-order scheme is used for spatial discretization.

2.1 Liquid phase solving

LES is adopted to simulate the carrier phase. The flow field is decomposed into large-scale motions and small-scale motions using a filter function. The larger three-dimensional unsteady turbulent motions are directly represented, whereas the effects of the smaller-scale motions are modelled[15]. The filtered continuity and momentum equations are as follows:

$$\frac{\partial \overline{u_i}}{\partial x_i} = 0 \tag{1}$$

$$\frac{\partial \overline{u_i}}{\partial t} + \overline{u_j}\frac{\partial \overline{u_i}}{\partial x_j} = -\frac{1}{\rho}\frac{\partial \overline{p}}{\partial x_i} - \frac{\partial}{\partial x_j}\left(\overline{\sigma_{ij}} + \tau_{ij}\right) + S_u + \frac{f_{pf}}{\rho} \tag{2}$$

where the overbar identifies filtered quantities. u_i is fluid velocity in three direction (i =x, y, z), ρ is the fluid density, p is pressure, σ_{ij} is viscous stress, τ_{ij} is the sub-grid scale stress tensor, which is required to close the equations. S_u represents the mean momentum source term, which is required to drive the channel flow. The SGS stress is modelled using Wall Adapting Local Eddy-Viscosity Model (WALE)[16]. The turbulent kinematic eddy-viscosity is defined as:

$$\nu_t = \left(C_w\Delta\right)^2 \frac{\left(S_{ij}^d S_{ij}^d\right)^{3/2}}{\left(\overline{S}_{ij}\overline{S}_{ij}\right)^{5/2} + \left(S_{ij}^d S_{ij}^d\right)^{5/4}} \tag{3}$$

where S_{ij} is the strain-rate tensor, Δ is the filter width. C_w is a constant, whcih is set to be 0.325 in the present study.

The effect of bubbles on the fluid is reflected in the last term of the Eq. (2). The hydrodynamic forces on all bubbles in each grid are added up and averaged by grid volume. According to Newton's third law, the coupling effect is achieved by apply the force to the fluid.

2.2 Discrete phase solving

Bubbles are assumed to be homogeneous spheres with constant diameters in this study. Collision between bubbles are considered but coalescence and breakup are ignored in the present work. Each bubble is tracked individually by solving the motion equation as follows:

$$m\frac{dv}{dt} = mg\left(1 - \frac{\rho_l}{\rho_b}\right) + \frac{3mC_D}{4d}\left|u - v\right|\left(u - v\right) + \frac{m\rho_l}{\rho_b}C_L\left(u - v\right)\times\left(\nabla\times u\right) + f_c \tag{4}$$

where the terms on the right side of Eq.(4) represent the gravity-buoyancy, drag force, shear-lift force, collide force, respectively. Drag coefficient C_D and lift coefficient C_L are determined by Tomiyama's drag model[17] and lift model[18] as follows:

$$C_D = \max\left(\min\left(\frac{16}{\mathrm{Re}}\left(1+0.15\,\mathrm{Re}^{0.687}\right),\frac{48}{\mathrm{Re}}\right),\frac{8}{3}\frac{Eo}{Eo+4}\right) \tag{5}$$

$$C_L = \begin{cases} \min\left[0.288\tanh\left(0.121\,\mathrm{Re}\right), f\left(Eo_d\right)\right] & Eo_d < 4 \\ f\left(Eo_d\right) & 4 \le Eo_d \le 10.7 \end{cases} \tag{6}$$

Previous studies usually ignored the interaction between bubbles[13] or used hard sphere model to simulate the collision[14]. However, it is the soft sphere model that can describe the bubble-bubble interaction and bubble-wall interaction more realistically. In this paper, a non-linear spring-dashpot-slider model is used to calculate contact forces. The normal and tangential contact forces can be obtained by:

$$f_c^n = -k_n\delta_n^{1.5} - \eta_n u_n \tag{7}$$

$$f_c^t = \begin{cases} -k_t\delta_t - \eta_t u_t & \left|f_c^t\right| < \mu\left|f_c^n\right| \\ -\mu\left|f_c^n\right| & \left|f_c^t\right| \ge \mu\left|f_c^n\right| \end{cases} \tag{8}$$

where k and η represent spring stiffness coefficient and damping coefficient, respectively. δ is overlap, u is the relative velocity, and μ is the friction coefficient. The subscript n and t represent the normal and tangential components, respectively. The spring stiffness coefficient is derived from surface tension σ as reference[19].

3 COMPUTATIONAL CONDITIONS

A turbulent channel flow laden with microbubbles is simulated. Dimension of the channel geometry and the coordinate system is shown in Figure 1 (a). In particular, the channel half height h is equal to 0.025m. The computational domain is discretized using grids in the streamwise, wall-normal and spanwise directions, respectively. The grids were distributed uniformly along the streamwise and spanwise directions, equal-ratio distribution is used for the wall-normal direction. Grid distribution can be seen in Figure 1 (b).

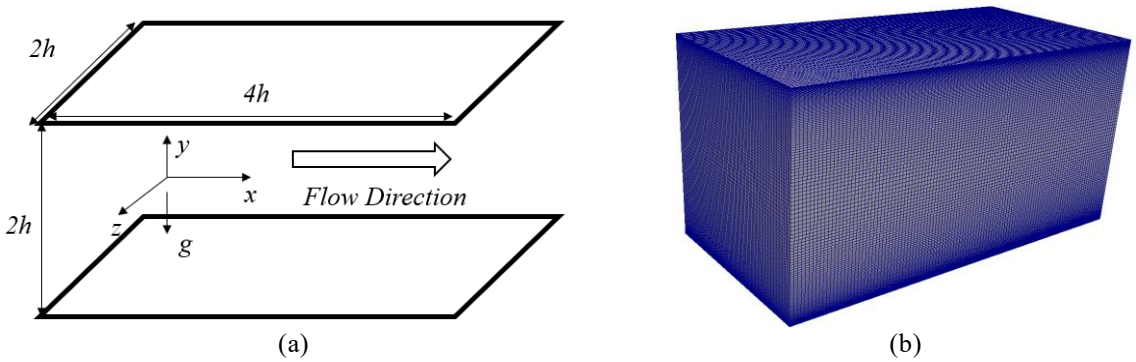

Figure 1: Computational domain and grid distribution. (a) Channel sketch. (b) Grid distribution.

Periodic boundary conditions are used in both the streamwise and spanwise directions for thee liquid flow to obtain a fully developed turbulent flow. At the same time, periodic boundary is also applied to microbubble motion to keep void fraction the same. No-slip boundary conditions are exerted on the channel top and bottom walls for the liquid flow, where mircobubbles will collide with the walls. The bubble-wall collision is solved by Eqn(7). Turbulent channel flow is developed with friction Reynolds number $\mathrm{Re}_\tau = 375$. At first, a single phase turbulent channel flow is obtained by long-time simulation. After a statistically steady state of the liquid-phase turbulence is reached, the microbubbles are injected into the channel uniformly. The density of bubble is set to 1.2 kg/m^3, and the bubble diameter is 110 μm. The corresponding total number of bubbles are 39366. The bubble volume fraction is choosen as $\alpha_b = 1.12\times10^{-4}$ refer to the literature[13][14], whcih has been proved large enough to have influence on the flow field. The initial velocity of microbubbles is equal to zero. Under these conditions, the interaction between liquid phase and microbubbles can be investigated by the bubble motion and turbulence changes.

4 RESULTS AND DISCUSSIONS

In this section, a fully developed single-phase turbulent channel flow is simulated firstly, and the turbulent flow field is validated by comparison with DNS results of Moser et al.[20]. Then, turbulent bubbly flow is simulated to investigate the interaction between microbubbles and turbulent flow.

4.1 Fully developed turbulent flow simulation

The evolutional process from laminar flow to turbulence in channel flow can be reproduced in a long time simulation with the use of periodic boundary conditions. Figure 2 shows the change of friction Reynolds number Re_τ with time and the corresponding flow field. The dimensionless time is defined as $t^+ = tu_\tau^2/\nu$.

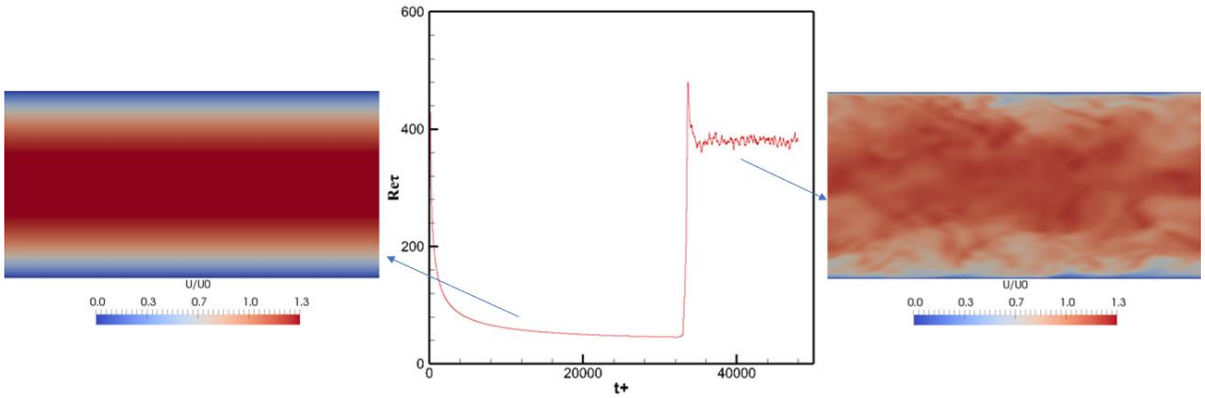

Figure 2: Time history of friction Reynolds number Re_τ and the corresponding flow field.

There is regular laminar flow in the channel for a long time at first as shown in the left figure in Figure 2. Frictional stress near the channel wall decreases with time. Then the

transition happens, frictional stress increase suddenly. The flow field begins to become disordered as shown in the right figure in Figure 2. The friction Reynolds number Re_τ oscillates around a fixed value. The flow field has become fully developed turbulence at this point.

The simulation of single phase turbulent flow is validated by comparison with DNS results of Moser et al.[20]. Figure 3 presents the comparison of mean velocity profile, while Figure 4 presents the comparison of turbulent intensities and Reynolds stress. These profiles have been obtained after averaging over time and space. The mean velocity profile shows good agreement with DNS results and the empirical formula. At the same time, the turbulent intensities and Reynolds stress are slightly under-predicted near the centre of the channel. It is worth noting that the simulation carried out by Moser et al.[20] is in the friction Reynolds number $Re_\tau = 395$, which is slightly larger than $Re_\tau = 375$ in the present work. It is the difference in Reynolds number that causes the difference in stress. In summary, the LES simulation has the ability to resolve the main characteristics of the turbulent flows.

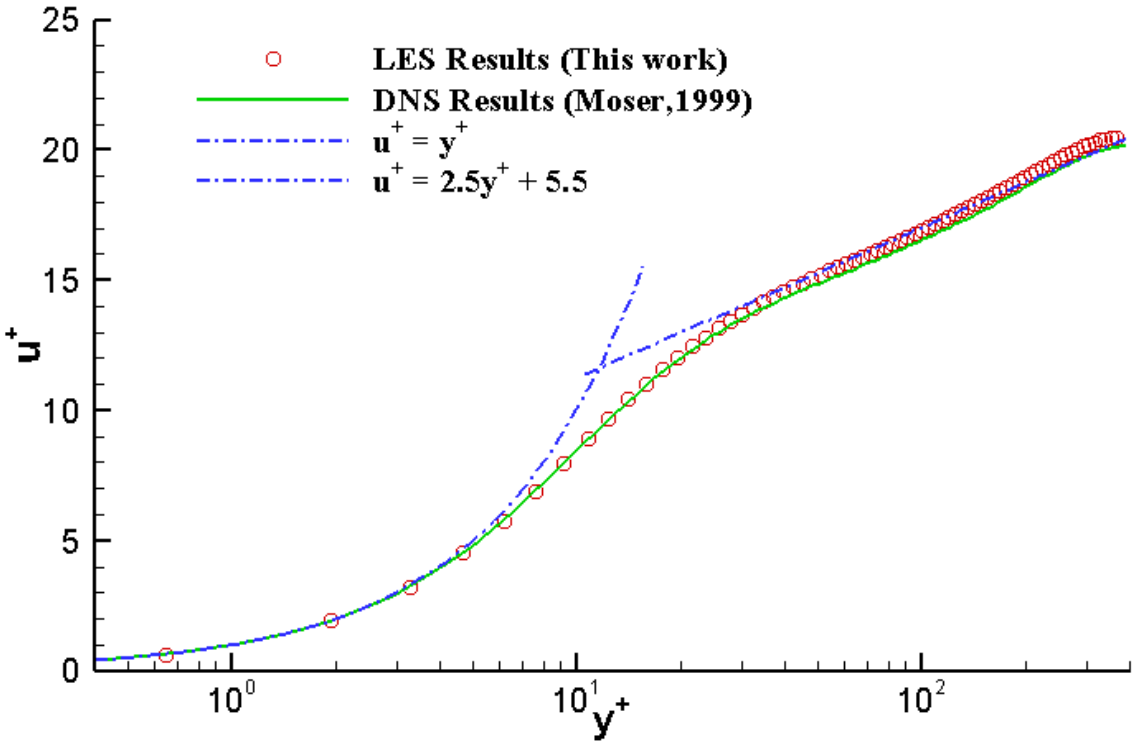

Figure 3: Comparison of mean velocity profile.

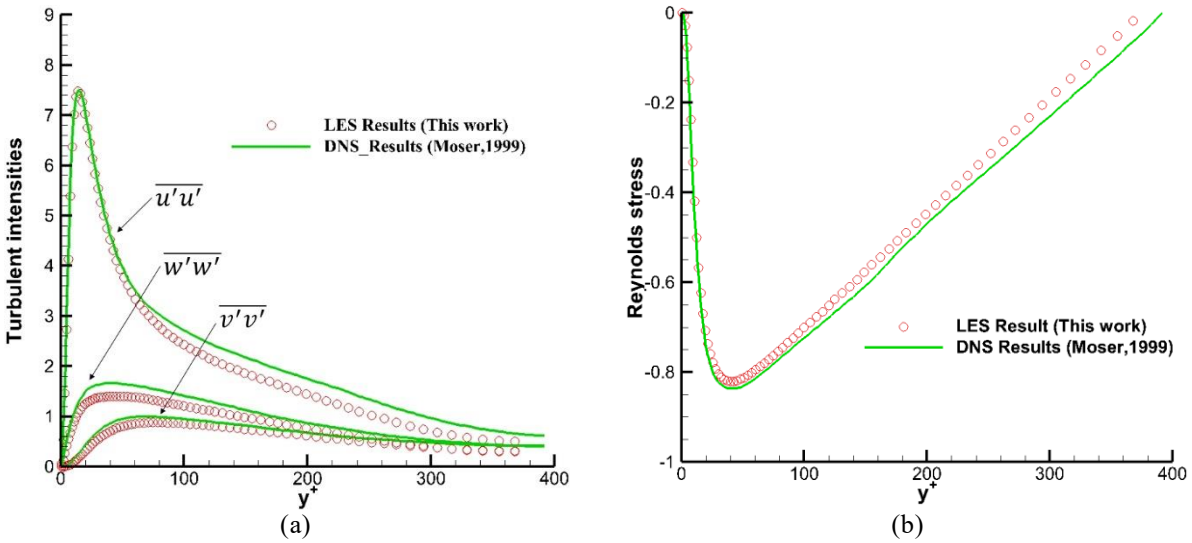

Figure 4: Comparison of turbulent intensities and Reynolds stress. (a) Turbulent intensities in three directions. (b) Reynolds stress

4.2 Bubbly channel flow simulation

In this section, the two phase coupled turbulent flow is simulated. Figure 5 presents the bubble transport process in the channel.

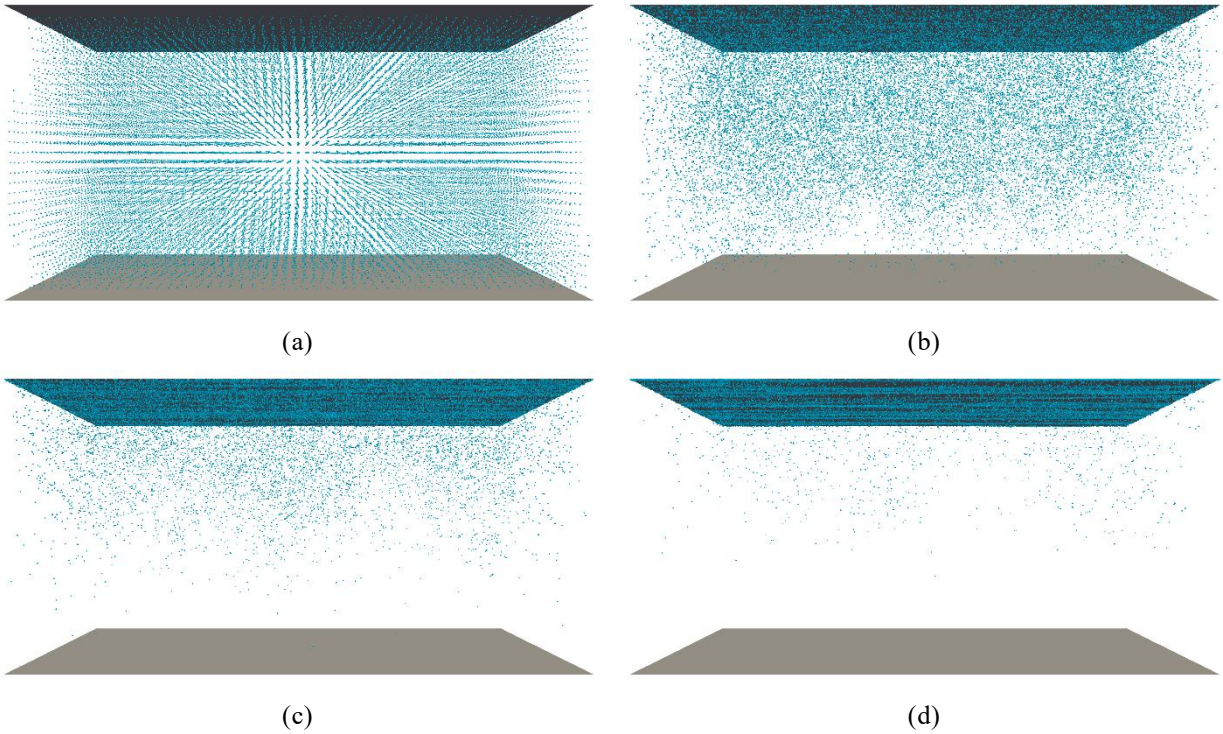

Figure 5: Microbubble transport process in the channel. (a) $t^+ = 0$ (b) $t^+ = 450$ (c) $t^+ = 1125$ (d) $t^+ = 1800$

After $t^+ = 1800$, most of microbubles have moved close to the upper wall. It can be concluded that gravity-buoyancy is the dominant force in the wall-normal direction. The bouyancy force from the large density difference leads to the floating motion of bubbles to the upper wall gradually. At the same time, the lift force on the bubbles also causes them to move towards the wall. On the other hand, drag force is the dominant force in the streamwise direction. After the bubbles are initialized with zero speed in the channel, they are affected by the drag force of the fluid to produce velocity in the flow direction, which is almost the same as the local fluid velocity. It is worth noting that not all the bubbles are sticking to the upper wall after the flow field reaches stability. There are still many microbubbles move towards or away from the wall in the turbulent boundary layer, which leads to the suppression of turbulent vortex and turbulent drag.

Figure 6 shows the time histories of steady state frictional drag coefficient τ_w^+ ($\tau_w^+ = \tau_w \Big/ \frac{1}{2}\rho u_\tau^2$) on the upper wall with and without microbubbles. In the steady state, drag force oscillates randomly around a fixed value. It can be seen that the existence of microbubbles results in a certain degree of drag reduction. Quantitatively, about 6% drag reduction effect is obtained. The effect is much larger than the drag reduction of Pang et al.[13] with the same bubble size and void fraction. The reason is that the microbubbles are considered to be as points in their paper, the change in viscosity of the mixed fluid was neglected. In this paper, The viscosity change is considered in the drag calculation. It can be probed from the results that the viscosity change caused by the microbubbles sticking to the wall can obviously improve the effect of drag reduction.

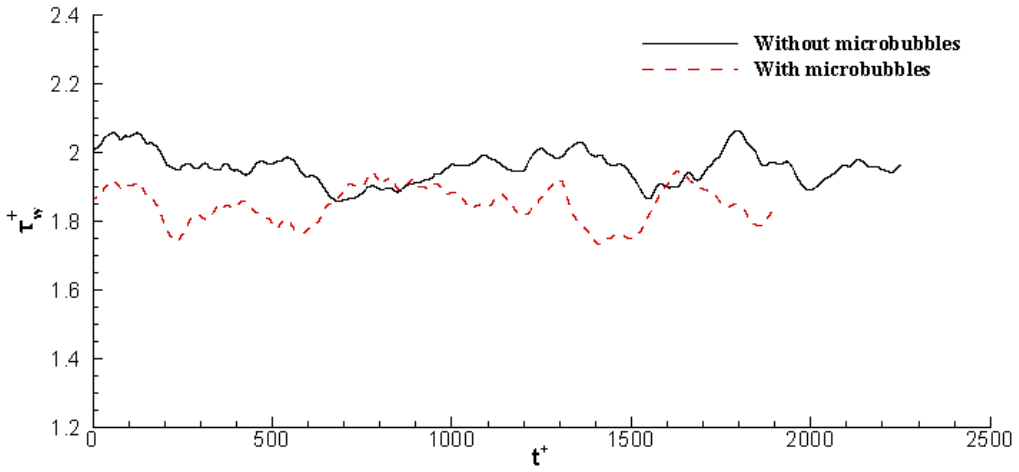

Figure 6: Time history of steady state frictional drag coefficient

Next, the influence of microbubbles on the turbulent flow is discussed in detail. The mean streamwise velocity profiles of the liquid phase with and without microbubbles are plotted in Figure 7. It is obvious that the mean velocity profile of the liquid phase with microbubbles displays a asymmetric shape in contrast with pure liquid flow. Specifically, the two profiles coincide completely in the lower half of the channel ($0 < y^+ < 375$), because there is no microbubble in that region. On the other hand, microbubbles concentrate in the upper half of the channel especially near the wall, which leads to a

squeeze on the fluid away from the wall. As a consequence, velociy near the channel centre is slightly higher than that in the pure liquid condition. At the same time, the velocity gradient near the wall is slightly decreases due to the presence of microbubbles, which contribute to drag reduction.

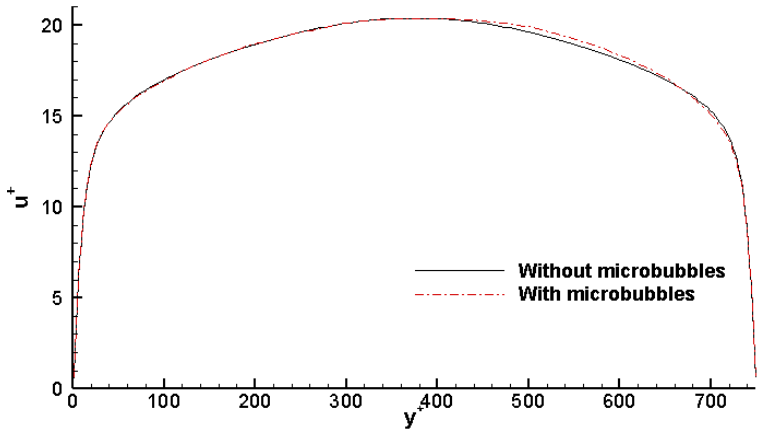

Figure 7: Mean velocity profiles of liquid.

Figure 8 presents the effect of microbubbles on the turbulent intensities and Reynolds stress in the upper half of the channel. It can be seen in Figure 8 (a) that the turbulent intensities of the liquid decrease by the impact of microbubbles. The decrease is more obvious in the wall-normal and spanwise directions, which indicates that microbubble has more obvious inhibitory effect on turbulent vortexes in the wall-normal and spanwise directions. The results are in qualitative agreement with the results of Pang et al.[13]. Figure 8 (b) shows that the distribution of Reynolds stress in the direction of channel height changes due to the presence of microbubbles. The magnitude of Reynolds stress decreases in the region near the wall ($y^+ < 250$). In the region away from the wall, Reynolds stress becomes slightly larger in the two phase flow than that in the single phase flow. In addition, the balance point is away from the channel center.

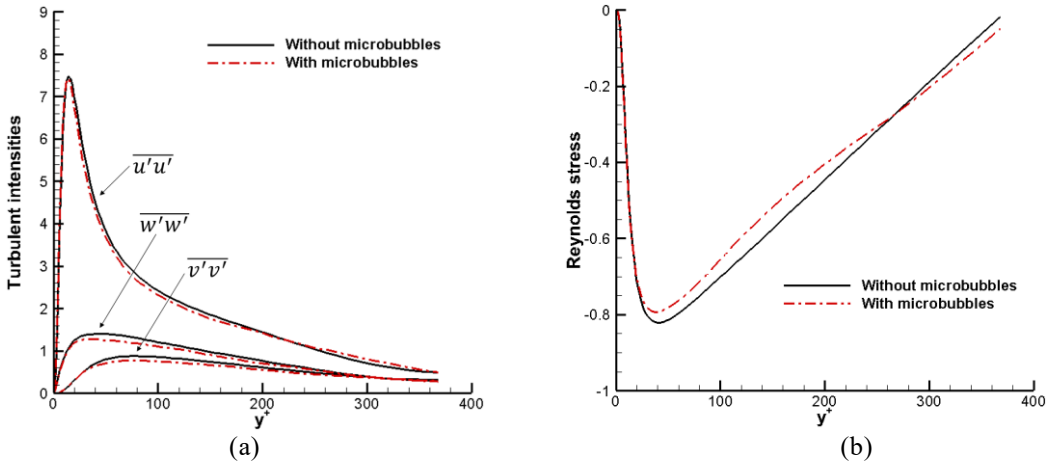

(a) (b)

Figure 8: Turbulent intensities and Reynolds stress. (a) Turbulent intensities in three directions. (b) Reynolds stress

5 CONCLUSION

In this paper, Euler-Lagrange method is used to simulate a turbulent channel flow with a large number of microbubbles. LES method is applied to capture the detail turbulent flow, while microbubble is tracked individually in Lagrangian framework. Interaction between liquid and microbubbles is solved. The simulation is carried out by the code developed base on OpenFOAM.

Firstly, a fully developed turbulent flow is simulated. Mean velocity profile, turbulent intensities and Reynolds stress are validated by comparison with DNS results. Then, microbubbles are injected into the channel. Bubbles moves towards the upper wall due to the action of buoyancy. About 6% drag reduction effect is obtained in the steady state. The drag reduction effect results from two aspects: On the one hand, microbubbles attached to the wall change the local viscosity. On the other hand, turbulent vortexes are inhibited by microbubbles in a certain degree. Both turbulent intensities and Reynolds stress decrease in the presence of microbubbles.

The drag reduction effect achieved in the present simulation is very limited. At the same time, there are also some unreal assumptions about the calculation conditions like the fixed bubble size. Future work will be focused on the simulation with larger void fraction, and the breakup and coalescence of bubbles will also be considered.

REFERENCES

[1] Fukuda, K., Tokunaga, J., Nobunaga, T., Nakatani, T., Iwasaki, T. Frictional Drag Reduction with Air Lubricant Over a Super-Water-Repellent Surface. *Journal of Marine Science and Technology*. (2000) **5**:123-130.

[2] Madavan, N. K., Detusch, S. & Merkle, C. L. Reduction of turbulent skin—friction by microbubbles. *Physics of Fluids*. (1984) **27(2)**: 356-363.

[3] Madavan, N. K., Detusch, S. & Merkle, C. L. Measurements of Local Skin Friction in a Microbubble Modified Turbulent Boundary Layer. *Journal of Fluid Mechanics*. (1985) **156**: 237-256.

[4] Merkle, C. L., Detusch, S. Microbubbles drag reduction. *Springer, Berlin, Gad-el-Hak M(ed) Frontiers in experimental fluid mechanics.* (1989) **46**: 291-335.

[5] Eric S., Winkel, Steven L., Ceccio, David R., Dowling. Marc Perlin Bubble-size distributions produced by wall injection of air into flowing freshwater, saltwater and surfactant solutions. *Experiments in Fluids*. (2004) **37**: 802-810.

[6] Sanders, W. C., Winkel, E. S., Dowling, D. R., Perlin, M. & Ceccio, S. L. Bubble friction drag reduction in a high-Reynolds-number flat-plate turbulent boundary layer. *Journal of Fluid Mechanics*. (2006) **552**: 353-380.

[7] Brian R. Elbing, Eric S. Winkel, Keary A. Lay, Steven L. Ceccio, David R., Dowling & Marc Perlin. Bubble-induced skin-friction drag reduction and the abrupt transition to air-layer drag reduction. *Journal of Fluid Mechanics* (2008) **612**: 201-236.

[8] Kunz, R. F., Deutsch, S., and Lindau, J. W. Two Fluid Modeling of Microbubble Turbulent Drag Reduction. *Proceedings of FEDSM'03: 4TH ASME-JSME Joint Fluids Engineering Conference*. (2003) Honolulu, Hawaii, ASME Paper No. FED2003-45640.

[9] Kunz, R. F., Gibeling, H. J., Maxey, M. R., Tryggvason, G., Fontaine, A. A., Petrie, H. L., Ceccio, S. L., Validation of two-fluid Eulerian CFD modelling for microbubble drag

reduction across a wide range of Reynolds numbers. *Journal of Fluids Engineering*. (2007) 129: 66-79.

[10] Shijie Qin, Ning Chu, Yan Yao, Jingting Liu, Bin Huang, and Dazhuan Wu. Stream-wise distribution of skin-friction drag reduction on a flat plate with bubble injection. *Physics of Fluids* (2007) **29**: 037103.

[11] Jin Xu, Martin R. Maxey and George Em Karniadakis. Numerical simulation of turbulent drag reduction using micro-bubbles. *Journal of Fluid Mechanics.* (2002) **468**: 271-281.

[12] Antonini Ferrante and Said Elghobashi. On the physical mechanisms of drag reduction in a spatially developing turbulent boundary layer laden with microbubbles. *Journal of Fluid Mechanics*. (2004) **503**: 345-355.

[13] M.J. Pang, J.J. Wei, B. Yu. Numerical study on modulation of microbubbles on turbulence frictional drag in a horizontal channel. *Ocean Engineering*. (2014) **81**: 58-68.

[14] Kenneth S. Asiagbe, Michael Fairweather, Derrick O. Njobuenwu, Marco Colombo. Large eddy simulation of microbubble transport in a turbulent horizontal channel flow. *International Journal of Multiphase Flow*. (2017) **94**: 80-93.

[15] Stephen B. Pope. Turbulent Flows. *Turbulent Flows*. (2000) 12, (11).

[16] F. Nicoud and F. Ducros. Subgrid-Scale Stress Modelling Based on the Square of the Velocity Gradient Tensor Flow. *Turbulence and Combustion*. (1999) **62**: 183-200.

[17] A. Tomiyama, G.P. Celata, S. Hosokawa, S. Yoshida. Terminal velocity of single bubbles in surface tension force dominant regime. *International Journal of Multiphase Flow*. (2002) **28**: 1497–1519.

[18] Akio Tomiyama, Hidesada Tamai, Iztok Zun, Shigeo Hosokawa. Transverse migration of single bubbles in simple shear fows. *Chemical Engineering Science*. (2002) **57**: 1849 – 1858.

[19] Van Hecke, M. Jamming of soft particles: geometry, mechanics, scaling and isostaticity. *Journal of Physics*. (2010) **22**: 3, 033101.

[20] Moser, R.D., Kim, J., Mansour, N.N. Direct numerical simulation of turbulent channel flow up to Re τ= 590. *Physics of Fluids*. (1999) **11**: 943–945.